JOURNAL OF PROPULSION AND POWER
Vol. 13, No. 3, May–June 1997

Counterflow Thrust Vector Control of Subsonic Jets: Continuous and Bistable Regimes

M. R. Van der Veer* and P. J. Strykowski†
University of Minnesota, Minneapolis, Minnesota 55455

Fluidic thrust vectoring of a subsonic jet was examined by the asymmetric application of counterflow to the jet shear layers. When counterflow is applied to one side of a 4:1 aspect ratio rectangular jet in the proximity of a control surface, the shear-layer entrainment characteristics are altered asymmetrically giving rise to a cross-stream pressure gradient and flow vectoring. Thrust vector control up to 20 deg was possible at Mach numbers up to 0.5 using counterflow. Two regimes of fluidic control were identified, a continuous regime and a bistable one. During continuous vectoring, proportional control could be achieved between jet response and the pressure conditions established in the counterflowing stream. However, under certain circumstances, proportional control was lost leading to jet bistability. Since such bistability is undesirable for aircraft control applications, the phenomenon was studied in detail. A parametric study of the collar geometry was used to minimize jet attachment and expand the operating domain over which proportional control could be maintained.

Introduction

THE redirection of the engine exhaust, namely thrust vectoring, may play a large role in the performance of the next generation of military aircraft. Thrust vector control has several advantages over maneuverability strategies based on aerodynamic control surfaces including poststall maneuvering, reduced takeoff distance and weight, and improvements in overall combat agility. However, many of the promising concepts currently under investigation require complicated hardware to vector the engine exhaust. This hardware typically consists of movable flaps and nozzles that can add considerable weight to the aircraft and can often be expensive in terms of added drag penalty, active cooling requirements, and time response. Here we will describe the operation of a fluidic thrust vectoring concept that relies on counterflow to redirect the jet exhaust. Fluidic thrust vectoring is based on fluid dynamic phenomena for control and has the potential advantage over existing technologies in that the control surfaces are stationary and are not directly exposed to the high-temperature exhaust gases. We will also examine the role of counterflow nozzle design on bistable jet operation that is known to limit the utility of many fluidic nozzle concepts.

Technology demonstrator aircraft employing first-generation vectoring nozzles have already proven the advantages of thrust vectoring under flight conditions.[1,2] These early vectoring nozzles have developed along two different lines: 1) rectangular, convergent–divergent nozzles with pitch vectoring and 2) axisymmetric jets with multiaxis vectoring capabilities. Two-dimensional vectoring was first tested on a modified F-15 aircraft fitted with twin-pitch vectoring nozzles, and demonstrated significant increases in pitch rate and reduced takeoff roll. Because of these proven performance enhancements and inherent low observable characteristics of rectangular nozzles, two-dimensional nozzles are being incorporated in the U.S. Air Forces' newest fighter, the F-22. Multiaxis thrust vectoring was first explored on the X-31 aircraft and on NASA's F/A-18 (HARV). The multiaxis vectoring capabilities of these first-generation systems were achieved by employing a simple system of three vanes arrayed around the nozzle exit. Even with these relatively simple systems, both the X-31 and F/A-18 demonstrated increased directional and lateral maneuverability with multiaxis thrust vector control. While these early flight demonstration nozzles proved the effectiveness of vectoring, aircraft integration issues such as weight, cooling and, particularly in the case of the vane systems, external drag, were of secondary concern. Estimates of these associated nozzle penalties, such as the studies done by Henderson[3] and Doonan and Kuchar,[4] will need to continue to fully assess the viability of new thrust vector concepts.

More recently, emphasis has been given to the development of high-performance multiaxis vectoring nozzles that attempt to retain the lightweight design of current axisymmetric nozzles, but allow deflection of the divergent section flaps in any direction through added actuation and control hardware. Most notable of these efforts were General Electric's AVEN nozzle[1,5] and Pratt and Whitney's P/Y BBN nozzle.[6] These axisymmetric exhaust systems are capable of vectoring up to 20 deg in pitch and yaw at rates exceeding 40 deg/s. These important studies indicate that multiaxis thrust vectoring can be successfully integrated into a production aircraft yielding benefits in enhanced maneuverability. Finally, although these multiaxis thrust vectoring nozzles are ideal for retrofitting current military aircraft, the AVEN and P/Y BBN would unlikely be integrated into future aircraft because of the relatively high radar cross signature of the round nozzle.

While vectoring jets using variable nozzle geometry is rapidly maturing, the use of fluidic nozzle design to achieve thrust vector control remains attractive owing to the potential elimination of heavy control and actuation hardware and the fast time response that fluidics can provide. Much of the early work on fluidic control was carried out in the context of fluid-jet amplifiers. Some studies[7–9] showed that small jets could be directed through the application of secondary air injection and auxiliary side walls at the jet exit. Since the primary purpose of these studies was to show the feasibility of such configurations for logic control devices, these fluidic control schemes were bistable in nature. Recently, Gilbert[10] showed that this technique could be applied on larger scales with high-pressure secondary air injected either perpendicularly or tangentially to the side walls. However, these techniques also suffered from bistable operation, being attached to either one wall or the

Received June 12, 1996; revision received Dec. 29, 1996; accepted for publication Jan. 21, 1997.

*Graduate Research Assistant; currently Senior Engineer, Teledyne Ryan Aeronautical, TCAE Turbine Engine Unit, Toledo, OH 43606.

†Associate Professor, Department of Mechanical Engineering. Member AIAA.

other with no proportional control of the vector angle, limiting their usefulness for aircraft control applications.

Fluidic thrust vectoring methods have also been tested on a larger scale for missile and aircraft control applications. One such scheme consisted of an overexpanded nozzle with control ports placed around the perimeter of the divergent section.[11,12] To vector the jet, one of the ports was vented to ambient air, leading to jet separation from that side of the nozzle resulting in vectored thrust. This technique requires that the ambient pressure is greater than the pressure in the divergent section of the nozzle; otherwise pressurized air was required. A related concept employs a chamber downstream of the convergent–divergent primary nozzle that reconverges to form an orifice.[13] Small amounts of pressurized air were injected into the confined chamber, forcing separation and redirection of the primary flow through the orifice. Although large thrust vector angles could be achieved in this manner, continuous control was possible only over a portion of the operating domain.

The aim of the present study is to examine a fluidic-based strategy, namely counterflow thrust vector control, which attempts to combine the continuous and proportional features of mechanical-based systems with the simplicity of fluidic control. The primary goals of this research are to achieve proportional and nonhysteretic control over a significant portion of the operation envelop, while minimizing the secondary mass flow required for actuation. The basic concept of counterflow thrust vector control can best be illustrated by referring to Fig. 1, where the side view of the short dimension of a rectangular jet is shown. The primary jet exhausts from the nozzle between curved surfaces, called collars, placed on either side of the primary stream. To achieve upward thrust vectoring at an angle δ_v, a secondary flow must be established in the upper shear layer of the jet. This can be accomplished by applying suction to the plenum chamber located between the upper curved surface and the primary nozzle. The action of counterflow in the upper shear layer gives rise to asymmetric entrainment and a cross-stream pressure gradient sufficient to vector the jet as shown in Fig. 1. The ability of the jet to vector in the presence of a stationary surface has been commonly referred to as the Coanda effect. The unique role of counterflow on jet entrainment and flow vectoring because of this Coanda effect, as well as the associated issue of bistable jet attachment, will be the focus of this study.

As a nominally two-dimensional jet issues from the nozzle, the shear between the jet and the surrounding quiescent fluid gives rise to lateral momentum transport, which is accentuated by the turbulent mixing of the shear layer. This process leads to momentum mixing between the two fluids and is commonly referred to simply as entrainment. Because the jet is gathering fluid through entrainment, its boundaries diffuse outward and, in the process, weaken the jet's ability to further entrain the surrounding fluid. Figure 2 depicts the two-dimensional jet with a curved surface of radius R aligned tangentially to the edge of the nozzle exit. The jet is seen to bend toward the curved surface. The mechanism responsible for this behavior has been described by several researchers.[14,15] The fluid entrained on the lower side of the jet is constrained by the presence of the curved surface. This surface requires that the entrained fluid be replaced by ambient fluid that must flow along the surface from downstream. For flow to enter this constricted region, the pressure there must be less than the pressure of the surroundings. This differential pressure draws the jet toward the curved surface. It is this change in the pressure field within the vicinity of a solid surface that is known as the Coanda effect. (First described by Young,[16] the Coanda effect is named for the French engineer who patented the effect in 1932.) If the entrainment rate is sufficiently high, the pressure continues to drop until the jet becomes attached to the surface. It is this attachment process that is most often associated with the

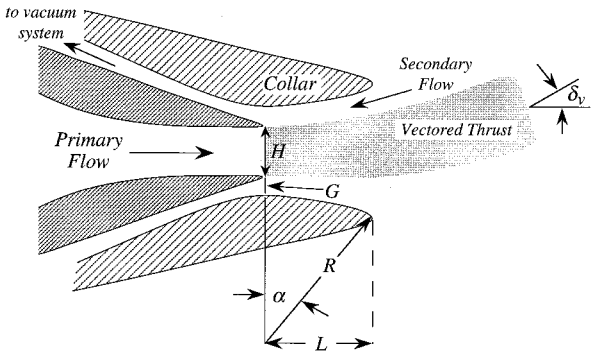

Fig. 1 Schematic of fluidic thrust vector nozzle showing vectoring when counterflow is activated in the upper shear layer of the jet.

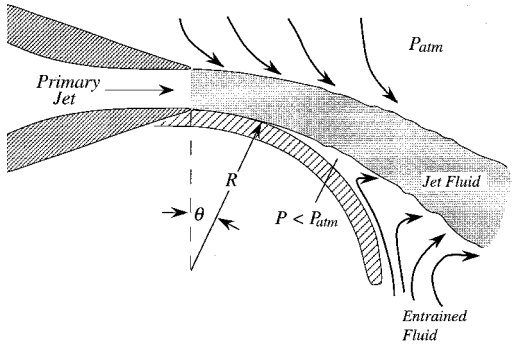

Fig. 2 Jet attachment to a curved surface caused by natural entrainment commonly referred to as the Coanda effect.

Coanda effect. However, attachment is not a necessary condition for the Coanda effect, but rather a consequence of it.

Once the flow becomes attached, the jet continues to entrain fluid between itself and the curved surface leading to further wrapping of the jet around the surface. This process continues until the shear-layer structures have weakened sufficiently and can no longer entrain the fluid necessary to force the jet against the surface. The point of separation of the jet from the surface is therefore dependent on the nature of the shear-layer structures and their ability to entrain ambient fluid. This observation is supported by the work of McGlaughlin and Greber,[17] which showed that the angle of attached flow separation depended highly on the jet turbulence. The turbulent jets, with their higher rates of entrainment, separated farther along the curved surface than did the laminar jets of the study. McGlaughlin and Greber[17] also showed that separation or attachment is influenced by nozzle geometry, with the higher aspect ratio jets more closely approximating two-dimensional flow and remaining attached farther downstream.

Once the jet has established itself in the configuration shown in Fig. 2 under steady conditions, it remains stable, i.e., perturbations to this flow result in the jet re-establishing itself to the condition prior to the perturbations. While the attached portion of the jet is obviously no longer entraining fluid against the curved wall, the pressure there is kept low as demanded by the equations of motion. Under these conditions, the curved jet can be described by two-dimensional cylindrical coordinates r and θ, which, respectively, are the local radius of the curved jet and its angular position. The corresponding local velocities in the r and θ directions are then u_r and u_θ. If we assume further that the flow is nominally parallel in the vicinity of the collar, namely that $u_\theta = u_\theta(r)$ and $u_r = 0$, we obtain for a steady, inviscid and incompressible fluid the following relationship:

$$\frac{\partial P}{\partial r} = \frac{\rho u_\theta^2}{r} \tag{1}$$

Consequently, the pressure gradient in the r direction is seen to increase with the square of the velocity. Therefore, the pressure will increase from some minimum value at the curved surface to atmospheric pressure near the outer boundary of the jet, ensuring that the centrifugal forces are balanced by the pressure field. The distribution of vacuum pressure maintained on the curved surface will determine the net forces acting on the surface. However, one of the inherent difficulties of controlling the Coanda effect, as described earlier, is its passive nature. For a given jet momentum flux and nozzle–collar geometry, a fixed pressure distribution will be created on the collar, and therefore a fixed side force will be generated. In this paper we consider whether these forces can be controlled in a proportional fashion to achieve continuous thrust vector control. Equation (1) suggests a deterministic relationship between the pressure gradient in the neighborhood of the collar surface and the radius of curvature of the jet. Consequently, if the jet curvature can be controlled by, for instance, manipulating jet entrainment, the cross-stream pressure field can be altered to generate the side forces necessary to vector thrust.

We continue this discussion in the next section by describing the jet facility and counterflow nozzle arrangement used during counterflow thrust vectoring. Subsequent sections will describe how the thrust vector angle is determined as well as identify both bistable and nonhysteretic regimes of thrust vector control using counterflow. The discussion will conclude with a summary of the physical mechanisms responsible for the fluidic control.

Facilities and Instrumentation

The primary jet velocity, denoted by U_1 in the jet exit plane, is established by passing air through a fifth-order polynomial nozzle having an area contraction ratio of approximately 20:1. The jet exhausts through a 4:1 aspect ratio rectangular exit, where H and W are the short and long dimensions of the jet exit, respectively. In the present study, the jet dimensions were held constant at $H = 1$ cm and $W = 4$ cm. The primary flow was driven by a constant-speed ring compressor providing steady operation over typical run times of 1–2 h. The tunnel stagnation pressure could be held to within 0.5% of its nominal value during this time period, providing jet exit Mach numbers up 0.5 (jet velocity of approximately 165 m/s). Because of significant heating of the air by the regenerative-type blower, a heat exchanger was used to maintain a constant stagnation temperature to within 0.3°C at a nominal value of 20°C. A Cartesian coordinate system was used with its origin located in the jet exit plane, with the x direction taken to be positive in the direction of the primary flow; the y and z axes were oriented along the short and long dimensions of the jet exit, respectively.

The secondary counterflowing stream was created by connecting a vacuum pump to the plenum formed between the curved collar surface and the primary nozzle as shown in Fig. 1. The magnitude of the reverse velocity U_2 was estimated by measuring the secondary mass flow in the vacuum system and assuming the velocity was uniformly distributed across the secondary flow path at $x = 0$. Hence, the secondary velocity U_2 is assumed to take a constant value in the gap defined by the height G. (The collars are placed symmetrically about the primary jet axis creating uniform gaps of G, both above and below the jet.) The curved collars define one boundary of the secondary flow path and consist of two parts: a flexible Teflon® portion that formed the plenum wall, and a rigid acrylic sectored arc having a constant radius of curvature R, and extending downstream of the primary jet exit a distance L. Since the collars were constructed of circular arcs, the radius of curvature and downstream extension length could be related through the turning angle α, where $L = R \cdot \sin \alpha$. Finally, parallel side plates spaced W apart and extending downstream a distance L, were used to confine the counterflow to either the upper or lower shear layer and thereby maintain a nominally two-dimensional flow. The jet two dimensionality was established through spanwise velocity surveys conducted downstream of the jet exit as well as through crossplane flow visualization; details of the two-dimensional nature of the flow can be found in the thesis of Van der Veer.[18]

The rigid portion of the collar wall could be interchanged with other sectored arc sections to affect changes in geometry. Collar lengths having $L/H = 1$, 2, and 3.5 were studied for turning angles of 30 and 60 deg. Furthermore, the secondary gap height G/H was variable between 0.2–1.0 through the use of adjustment screws. Each collar was carefully machined to accommodate surface static pressure taps along the centerline of the collar, which were used to evaluate the force distribution on the collar. The first tap was located at $x = 0$ and indicates the static gauge pressure in the gap of the secondary stream and will be denoted by P_G. A summary of the nozzle–collar parametrics examined during the course of this study are provided in Table 1.

A study was initially conducted to determine the influence of the collar surfaces on jet entrainment in the absence of counterflow. The characteristics of the rectangular freejet were examined in the streamwise direction by removing the collar surfaces and allowing the free entrainment of surrounding ambient fluid. The freejet data were compared to mean velocity measurements made in the jet when the collars were positioned downstream of the nozzle, but the vacuum system was turned off, thereby isolating the effect of the collar surfaces on the jet in the absence of counterflow. The data in Fig. 3, obtained at downstream distances between $x/H = 10$ and 40 at a Mach number of 0.5, indicate that the presence of the collar itself plays a very minor role in effecting the streamwise jet evolution when counterflow is not applied to the jet shear layers. The results of this initial condition study were relatively insensitive to the precise collar geometry given in Table 1, but did depend somewhat on the gap height between the jet and collar, G/H. The measurements in Fig. 3 were taken at $G/H = 0.2$, which was the smallest gap height examined during the course of this study and had the most noticeable affect on the jet development, which can be seen from Fig. 3 to be quite insignificant. Measurements to be presented later in this paper

Table 1 Collar configurations examined in this study

Collar	L/H	α, deg	R/H
1	3.5	30	7.0
2	2.0	30	4.0
3	1.0	30	2.0
4	2.0	60	2.3

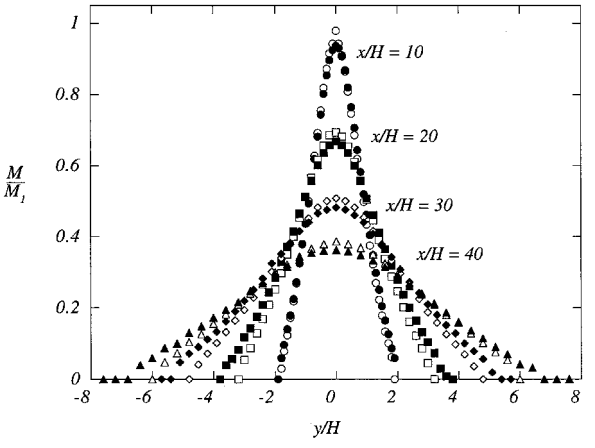

Fig. 3 Mach number profiles comparing the jet development with (solid symbols) and without (open symbols) the presence of a collar surface. Profiles were taken at $M_1 = 0.5$ for collar no. 3.

will demonstrate that although jet spreading is not affected by the presence of the collar alone, jet spreading is significantly influenced by the presence of the collar surfaces when counterflow is applied to the jet shear layer.

Experimental Procedure

One of the principal measurands sought in the present problem is the resultant thrust vector angle δ_v, shown graphically in Fig. 1, and its functional dependence on the amount of counterflow applied to the jet shear layer. In the absence of a direct measurement of jet performance using a thrust stand, the vectored thrust was evaluated by two independent methods. One estimate of δ_v was obtained from measurements of the velocity field downstream of the nozzle–collar assembly where jet curvature was negligible and the local static pressure was equal to ambient pressure. This was accomplished by positioning a standard pitot tube on an automated traversing system and obtaining cross-stream pitot pressure profiles at many streamwise positions in the jet. This procedure simply required that the pitot was aligned with the direction of the vectored jet, which was accommodated by positioning the pitot on a turntable having an angular resolution of 1 deg. Some iteration was required to assure that the pitot was accurately aligned with the flow direction, a precaution that was used despite the insensitivity of the pitot to approach angles less than approximately 10 deg. Analysis of the profile evolution in the streamwise direction could be used to obtain estimates of δ_v. This was possible sufficiently downstream of the jet exit where the profiles displayed a nearly symmetric behavior. Because of its repeatability, this method was used throughout the study, but because the method was very time intensive, a control volume estimate of δ_v was also used as described next.

The most unambiguous definition of δ_v can be obtained by considering a control volume that includes the jet exit plane, the collar and external surfaces, and extends upstream of the nozzle-collar assembly sufficiently far so that the pressure on the boundary of the control volume can be considered atmospheric and the integrated momentum flux can be neglected. This control volume necessarily contains a net reaction force required to support the assembly that can be resolved into the Cartesian components R_x and R_y. The thrust vector angle can then be defined as $\delta_v = \tan^{-1}(R_y/R_x)$. In the absence of a thrust stand, the resultant forces are obtained by measuring the static pressure distributions on the collar and nozzle assembly and the primary/secondary stream momentum fluxes as they cross the control volume. The pressure distribution on the active collar was integrated to determine the axial and transverse collar forces. Pressure measurements were also made on the inactive collar (side opposite to the collar where counterflow was applied), but the magnitude of these forces was always less than ~0.5% of the forces on the active collar, and so they could be reasonably neglected. The pressure force exerted on the gap plane, labeled as G in Fig. 1, was estimated by assuming that the collar pressure P_G was distributed uniformly across the secondary flow gap; the pressure across the primary jet at $x = 0$ was assumed to be uniform and equal to ambient pressure. As discussed earlier, U_2 was obtained by assuming that the mass flux drawn into the vacuum system was distributed uniformly across the gap at $x = 0$. Viscous forces were neglected in the analysis.

Precision and bias error estimates in measured quantities were propagated through the data reduction equations to evaluate first-order uncertainties at 95% confidence. The relative uncertainty in the thrust vector angles obtained from the control volume analysis was estimated to be less than ±2%; the relative uncertainties in collar forces and momentum fluxes used to evaluate δ_v were less than ±0.5 and ±1.5%, respectively. Error propagation was also used to evaluate the uncertainties in velocity and mass flow ratios. Nominal values for the uncertainties in $-U_2/U_1$ and $\dot{m}_2/\dot{m}_1$ were ±0.015 and ±0.005, respectively. Collar static pressures were evaluated to have relative uncertainties better than ±0.2%.

Results and Discussion

The jet response to counterflow can be seen quite clearly in Fig. 4, where the thrust vector angle is shown as a function of vacuum pressure $-P_G$ in the secondary stream measured at $x = 0$. Vector angles indicated by solid symbols were evaluated by using the control volume method and the open symbols were obtained by examining pitot pressure profiles in the jet downstream of the nozzle-collar assembly. The agreement between the two approaches suggests that the assumptions employed in the control volume momentum balance were reasonable.

The thrust vector response curve shown in Fig. 4 predicts a nearly linear relationship between δ_v and vacuum pressure in the secondary flow path over the range of conditions studied. The data fall into two categories. On the lower portion of the curve, the jet could be vectored continuously from 0 deg to ~20 deg in a very repeatable manner. The upper portion of the curve shows a cluster of data points at a vector angle of nearly 50 deg, a value that was determined by geometric constraints of the collar, as discussed later. Stable thrust vector control was not possible in the domain between the two data sets, namely for $-P_G$ between approximately 50–95 torr.

The gap in the data was a consequence of the bistable jet behavior that can best be observed by replotting δ_v vs mass flow ratio $\dot{m}_2/\dot{m}_1$ (see Fig. 5). The most striking characteristic of this plot is the hysteresis loop that is formed by the data. At low levels of counterflow, the thrust vector angle increases monotonically with secondary mass flow rate. However, as the vector angle increases, the jet moves closer to the collar surface, thereby reducing the area through which the secondary flow may pass. Hence, a decrease in secondary mass flow rate can be seen when δ_v exceeds ~10 deg. Eventually, the pressure between the primary jet and the collar wall becomes sufficiently low so that the jet can no longer remain stably on the lower portion of the curve of Fig. 5, and the jet abruptly attaches to the collar, increasing the thrust vector angle to ~50 deg while significantly decreasing the secondary mass flow rate. In this situation the jet follows the upward arrow in Fig. 5, a condition resulting in jet attachment. When the jet assumes the attached configuration, the secondary mass flow is drawn almost entirely from the primary jet. Since the radius of curvature of the jet necessary to establish attached conditions is significantly smaller than that for unattached conditions, the vacuum pressure is increased during attachment as anticipated by Eq. (1).

Once the jet is attached to the collar, closing the valve between the secondary plenum and the vacuum pump from its position prior to attachment has no noticeable effect on jet response. The jet will remain stably attached to the collar until

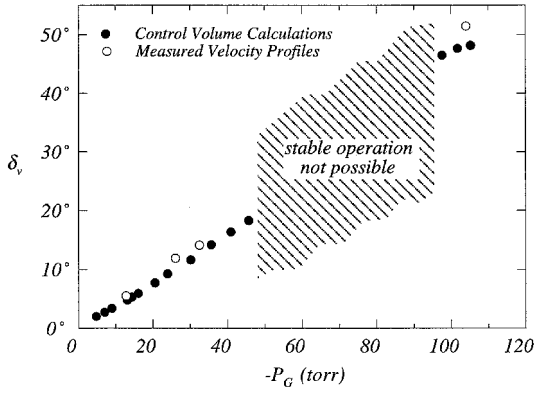

Fig. 4 Thrust vector response curve as a function of gap pressure in the secondary stream. Data were obtained at $M_1 = 0.5$ for collar no. 4 with $G/H = 0.4$.

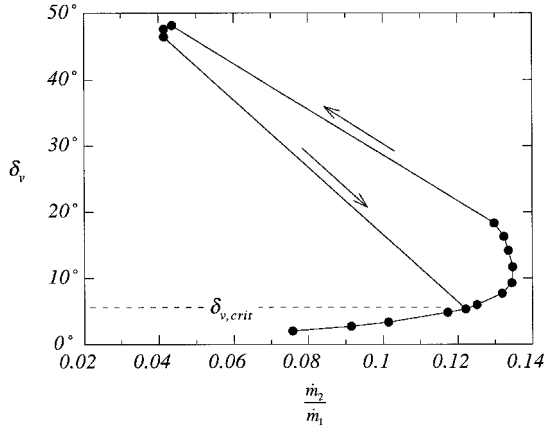

Fig. 5 Thrust vector response showing hysteresis effects and critical δ_v. Data were obtained at $M_1 = 0.5$ for collar no. 4 with $G/H = 0.4$.

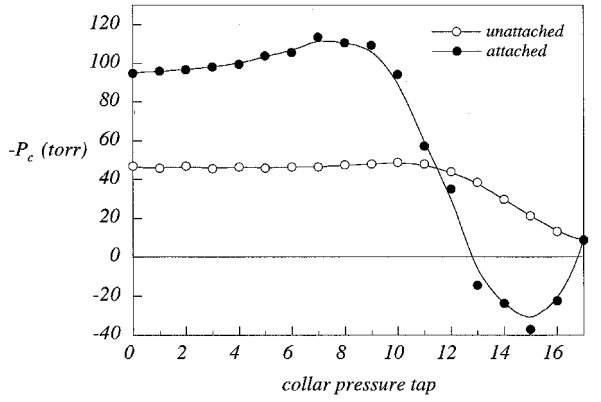

Fig. 6 Collar static pressure distributions for unattached and attached flow conditions using collar no. 4 with $G/H = 0.4$ and at $M_1 = 0.5$.

the valve is considerably closed to the point where the primary jet momentum can overcome the vacuum pressure created by the pumping action of the primary jet itself. At this point the jet releases from the collar surface, establishing a new equilibrium condition on the lower curve following the downward arrow in Fig. 5. This intersection will be called the critical vector angle $\delta_{v,crit}$, indicating the maximum angle that can be achieved in the absence of hysteresis effects. Since the control valve was closed considerably to facilitate jet detachment from the collar, the jet reaches equilibrium on the lower curve at a relatively small angle of about 6 deg in Fig. 5. Hysteretic behavior of this nature is quite reminiscent of fluidic jets.[10]

The loop defines a bistable regime where the jet is either controlled continuously with counterflow (lower curve) or remains fixed to the collar surface (upper curve). The precise position along the lower curve where the jet will jump to the upper curve is a function of the disturbance level experienced by the jet. The upward arrow in Fig. 5 is not unique, but simply the route taken when the valve is opened slowly. The critical vector angle, however, defines the angle below which disturbances of any amplitude will not cause jet attachment. Clearly, collar designs must be considered that can increase $\delta_{v,crit}$ while decreasing the secondary mass flow requirements needed to achieve a particular nonhysteretic operating point. The behavior shown in Fig. 5, while not optimal, serves to illustrate the basic phenomena that we observed for all collars tested over Mach numbers ranging from approximately 0.3–0.5. As will be shown in the results to follow, the performance of the system is highly dependent on the nozzle–collar geometry, which can be optimized for specific applications.

Further insight into the attached jet behavior can be obtained by examining collar pressure distributions prior to and during attachment. Figure 6 shows attached and unattached collar pressure profiles for collar no. 4. Both unattached and attached profiles vary smoothly from P_G at the first tap location ($x = 0$) to atmospheric pressure at the downstream extent of the collar (pressure tap no. 17). To sustain jet attachment and vector angles of ~50 deg, the vacuum pressure during attachment is quite large. The pressure distribution during attachment indicates a relatively constant pressure near the jet exit, marking the portion of the collar wall within the separation bubble formed behind the attached jet. This bubble consists of relatively low kinetic energy fluid diverted from the primary jet flow. Downstream of this bubble, the fluid in the jet shear layer near the wall is decelerated and recovers a portion of its available stagnation pressure, giving rise to a local maximum in absolute pressure. This pressure maximum identifies the approximate location of the attaching streamline. Downstream of attachment, the flow accelerates along the curved surface as the pressure adjusts to atmospheric conditions at the termination of the collar; the pressure at the final tap does not achieve atmospheric pressure because of the subtle streamline curvature of the flow in this region of the collar. By contrast, the collar pressure distribution for the unattached flow varies continuously from the vacuum conditions at $x = 0$, to nearly atmospheric pressure at the farthest downstream pressure tap no. 17.

Thrust Vector Control: Unattached Flow

From a practical perspective attached flow conditions would be unacceptable for aerodynamic control applications. For that reason we concentrated our efforts on the continuous portion of the operating curve and examined the parametric effects involving collar geometry to determine whether the critical vector angle could be increased. In particular, we examined the influence of collar length L/H and offset distance G/H as the primary geometric parameters in the problem; the collar geometries considered here are listed in Table 1. We also examined the scaling of the unattached thrust vector performance over the range of Mach numbers between 0.3–0.5.

Collar length must play an essential role in the performance of a counterflow thrust vector nozzle, since the side loads required to vector thrust must be distributed along the curved portion of the jet shear layer that extends downstream of the jet exit a distance approximately equal to L. Here we considered collars no. 1, 2, and 3 from Table 1, which varied in length from $L/H = 1–3.5$ for a fixed turning angle of $\alpha = 30$ deg. The data, which were acquired over a wide range of collar offset heights, collapse onto three curves representative of each collar length, as shown in Fig. 7. It is important to note that the collar offset height G/H had essentially no effect on vector performance when viewed as δ_v vs P_G. (Note that although gap height does not play a significant role in determining vector response, it does affect the secondary mass flow rate needed to achieve a particular thrust vector angle. This will be discussed in greater detail later.) The most significant feature of Fig. 7 is that, for a given vacuum pressure, larger vector angles can be achieved with longer collars. This is not surprising since increasing L will increase the total side force on the collar for a fixed differential pressure across the collar. Since the magnitude of P_G is indicative of the overall collar pressure distribution, as seen by the unattached profile in Fig. 6, the resultant normal collar force is proportionally greater for a longer collar. Conversely, a longer collar is capable of achieving a desired value of δ_v at a smaller vacuum pressure.

The data in Fig. 7 correspond to the continuous thrust vector response curves that may display hysteretic behavior, depending on the value of $\delta_{v,crit}$, as discussed in conjunction with Fig. 5. The thrust performance will only be unique and nonhysteretic at thrust vector angles less than $\delta_{v,crit}$. Determination of the critical angle requires that jet attachment first be established, and then the vacuum control valve altered to allow the release

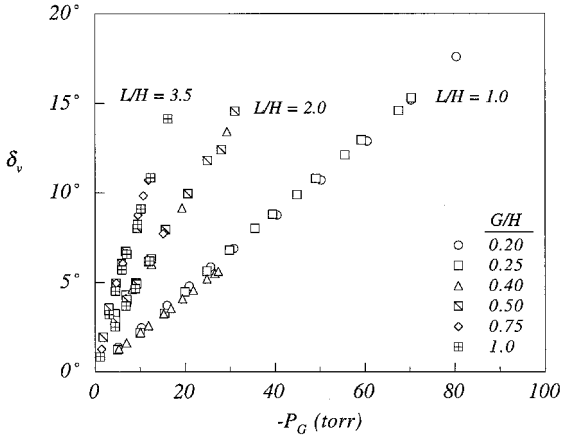

Fig. 7 Thrust vector response curves for collars no. 1, 2, and 3 at $M_1 = 0.5$. Jet response shows dependence on L/H and insensitivity to G/H.

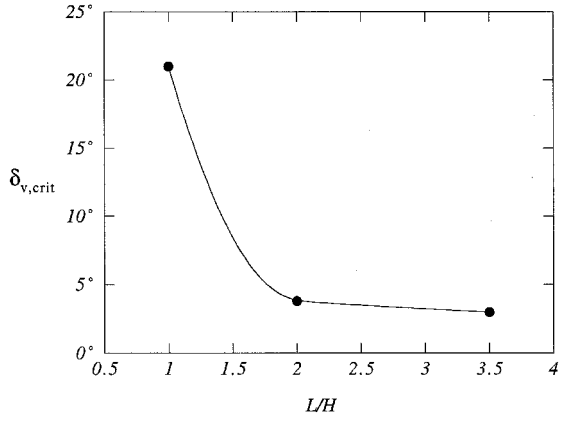

Fig. 8 Critical vector angle for collars no. 1, 2, and 3 at $M_1 = 0.5$.

of the jet from the collar surface. The resulting critical thrust vector angles are plotted in Fig. 8 for the three collars examined in this study having turning angles of $\alpha = 30$ deg. The data indicate that $\delta_{v,crit}$ is quite insensitive to collar length when L/H is greater than approximately 2, but strongly dependent on collar length for small values of L/H. Large values of $\delta_{v,crit}$ are extremely desirable for aircraft vectoring, and we could anticipate that $\delta_{v,crit}$ must increase with decreases in L/H, since in the limit of $L/H \rightarrow 0$ jet attachment would be very difficult. Finally, we should point out that the data in Fig. 8 were obtained over collar gap heights G/H between 0.2–0.5. No noticeable dependence on gap height could be observed over this range of G/H, suggesting that the radius of curvature of the jet, under the conditions present when the jet releases from the collar, does not vary appreciably with collar offset.

The role of collar offset height G/H was also examined as an independent geometric parameter in this study. A flexible Teflon section was used to connect the rigid acrylic collars to the secondary flow plenum, and thereby assure a smooth transition over the full range of movement of the collar. To examine the role of secondary flow gap more carefully, δ_v was plotted as a function of $\dot{m}_2/\dot{m}_1$ over a range of G/H between 0.25–0.6. The curves shown in Fig. 9 only indicate the continuous portion of each operating curve. The attached flow portion of the hysteresis loop was omitted here for clarity, but would be located near $\delta_v \sim 50$ deg, as indicated by the upward arrows in Fig. 9. (For comparison purposes, the data for $G/H = 0.4$ from Fig. 5 are replotted in Fig. 9.)

The most apparent feature of the curves in Fig. 9 is that for increasing gap height, more reverse flow is required to attain a given thrust vector angle. In fact, a closer look at the data reveals that the secondary mass flow rate increases nearly proportionally to the increase in G/H, suggesting that δ_v may scale more universally on the velocity ratio $-U_2/U_1$. The data from Fig. 9 were replotted as a function of $-U_2/U_1$ in Fig. 10, by normalizing each curve by its respective gap height. While the curves do not collapse precisely, there appears to be some evidence that the velocity ratio is the controlling parameter, and that $\dot{m}_2/\dot{m}_1$ enters the problem only through its scaling with G/H. Some of the scatter in the data of Fig. 10 may be attributed to subtle differences in the shape of the velocity field in the countercurrent shear layer caused by variations in the gap height. (The density ratio between the primary and secondary streams was assumed to be unity for the purposes of this exercise. Although this is strictly not true for a primary stream Mach number of 0.5, where the density ratio differs from unity by approximately 5%, the scatter in the data of Fig. 10 will not be affected by this incompressible assumption since the density ratio is constant. The role of density ratio will be more pronounced at higher jet Mach numbers, as discussed at the end of this paper.)

To eliminate uncertainties caused by geometric variations, a similar set of measurements was taken with the collar geometry held fixed and the primary jet velocity varied. These data, shown in Fig. 11, were obtained over a Mach number range of 0.32–0.5, corresponding to an increase in forward jet velocity from 110 to 170 m/s. The measurements show, quite convincingly, that a unique velocity ratio can be associated with a particular thrust vector angle. Presumably, the velocity ratio plays an important role in determining the entrainment characteristics of the shear layer in the neighborhood of the

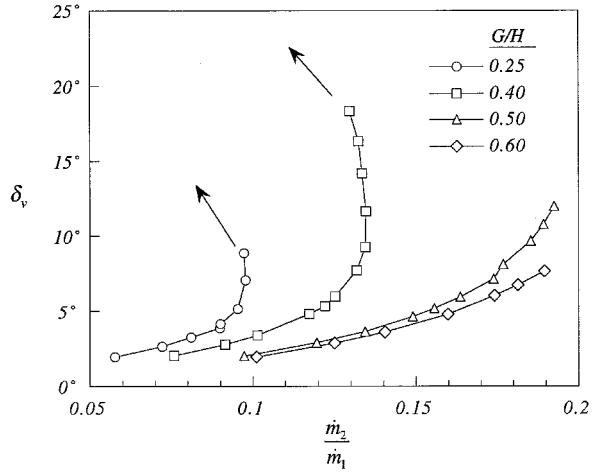

Fig. 9 Jet response to secondary mass flow and offset height G/H. Data were obtained for collar no. 4 at $M_1 = 0.5$.

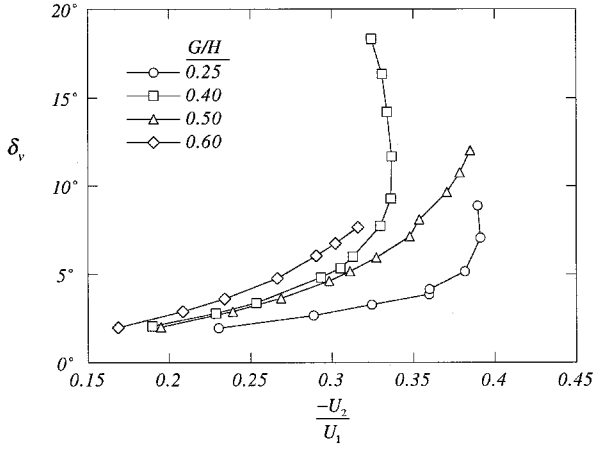

Fig. 10 Jet response to velocity ratio for collar no. 4 at $M_1 = 0.5$.

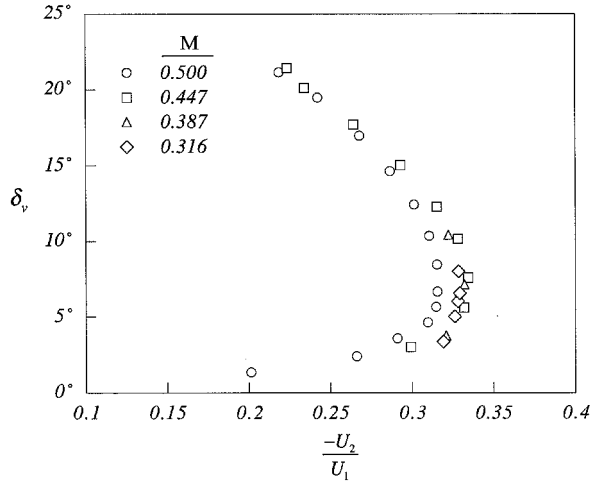

Fig. 11 Thrust vector response showing dependence on velocity ratio for collar no. 3 and variable Mach number. Gap height was G/H = 0.2.

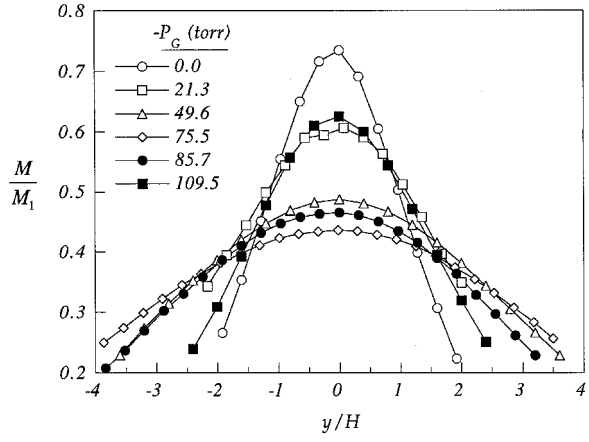

Fig. 12 Mach number profiles showing the initial increase in jet mixing, the subsequent decrease in mixing as the jet approaches the collar surface. Data were obtained at x/H = 16 for collar no. 3 with G/H = 0.2 and at M_1 = 0.5.

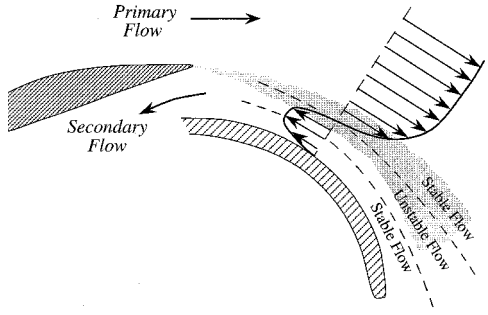

Fig. 13 Diagram showing the centrifugal instability of the countercurrent mixing layer in the proximity of a curved surface.

collar, much in the same fashion that was shown in unbounded coflowing[19] and counterflowing[20] shear layers. Although the maximum velocity ratio of nearly 33% indicated in Fig. 11 is quite high, an optimal collar design would seek to minimize the offset height to reduce external drag on the nozzle–collar assembly, which in turn, would decrease the pumping requirements by reducing the secondary mass flow ratio.

The connection between $-U_2/U_1$ and δ_v requires careful consideration. Counterflow in conjunction with collars has been shown to be an effective means of enhancing the mixing of freejets with turbulent shear layers in both the incompressible and compressible flow regimes.[20,21] These studies showed that a countercurrent mixing layer allowed the formation of large three-dimensional structures within the layer. These structures enhanced the entrainment of the shear layer, which led to elevated growth rates as velocity ratio $-U_2/U_1$ was increased. When counterflow is applied to one shear layer of the rectangular jet in this study, the resulting structures will augment the entrainment of mass. This process will be inhibited by the presence of the collar, resulting in reduced pressures on and in the vicinity of the collar surface, and thereby drawing the jet off-axis. Unlike the passive Coanda effect described earlier, however, the amount of entrainment and, thus, the pressure field, can be controlled by adjusting the velocity ratio. In this way the thrust vector angle can be controlled in a continuous fashion.

Evidence of enhanced mixing with the application of counterflow to the jet is seen in Fig. 12. The figure shows cross-stream Mach number profiles taken at a fixed distance downstream of the collar for different levels of counterflow. As the vacuum pressure is increased, the profile spreads out laterally, indicating increased jet mixing with $-U_2/U_1$. The spreading reaches a maximum at an exit gauge pressure of approximately −76 torr, and then decreases as suction is further increased. We believe this nonmonotonic behavior is caused by the jet proximity to the wall, which restricts the lateral scale of the shear-layer structures and thus the spreading rate of the jet farther downstream. Eventually, as the jet approaches the wall, the free shear layer of the jet undergoes a transition to a wall-bounded countercurrent layer, the dynamics of which have not been studied to our knowledge. The velocity field in the neighborhood of the curved surface must have a time-averaged profile of the type shown in Fig. 13, where the velocity increases radially outward except in a small region located away from the wall. Rayleigh's criterion for the centrifugal instability of inviscid fluid would suggest that this intermediate region is inherently unstable since the local circulation decreases radially outward.[22] Consequently, we can anticipate that a mechanism exists for destabilizing this wall-bounded flow, even as the primary fluid moves very close to the collar surface.

Continuous control of the jet can be maintained without jet attachment, in principle, for the following reason. The vectoring of the jet will reduce the cross-sectional area of the counterflowing channel (the area between the jet shear layer and the collar wall), thus increasing the pressure drop in the secondary stream. Consequently, the amount of counterflow will be reduced and with it the generation of the shear-layer structures required for additional entrainment. An equilibrium position will be achieved where sufficient suction is present to excite the layer and cause vectoring, but not too large a vector angle such that the entrainment because of the counterflow is cut off. By contrast, during jet attachment, there exists sufficient vacuum pressure to hold the jet against the collar in the absence of counterflow. When these conditions are present, continuous control of the pressure field is lost, leading to a bistable jet response. However, as described earlier, given a short enough collar, continuous control of the vectoring jet can be maintained to angles over 20 deg. The ability to control jet mixing and entrainment through continuous variation of the velocity ratio is responsible for the proportional thrust vector control and a key to the success of the technique.

Thrust Vector Design Law

During the course of this study, continuous thrust vector control was achieved over a range of flow conditions and using a variety of nozzle–collar geometries. Using these data and a simple scaling law, we attempted to develop a design curve that could be used to predict the counterflow thrust vector performance at conditions not explicitly examined as a part of this study. The relevant scaling parameters can be argued by referring to the sketch in Fig. 1. If we model the jet as nominally parallel in the region encompassed by the collars, then

the radial pressure gradient developed across the uniform jet column can be estimated using Eq. (1), namely: $\partial P/\partial r = \rho u_\theta^2/r$. We can estimate $\partial P/\partial r$ as the ratio of the differential pressure across the jet ΔP ($\approx -P_G$) and the jet width H. The term ρu_θ^2 is the jet exit momentum flux and is divided by the average radius of curvature of the jet, which for relatively small vector angles can be assumed to be constant and equal to R'. With the understanding that the jet will cease to deflect after departing the collar at a length L, we can use the geometric relation that $L = R' \cdot \sin \delta_v$, and show that

$$\sin \delta_v = \frac{-P_G}{\rho U_1^2} \cdot \frac{L}{H} \tag{2}$$

In effect, Eq. (2) is the ratio of the side force experienced on the jet shear layer to the axial force imposed by the jet.

All data gathered in the continuous thrust vector regime were normalized using the scaling suggested by Eq. (2) and are plotted in Fig. 14. The data constitute primary jet Mach numbers between 0.3–0.5 for the collar geometries given in Table 1. (Collar lengths L/H between 1–3.5, gap heights G/H from 0.2 to 1.0, and turning angles of 30 and 60 deg.) Despite some scatter in the data, the pressure parameter forming the abscissa in Fig. 14 captures the wide range of conditions examined in this study quite adequately; as a means of comparison, the model Eq. (2) is plotted as the solid line in Fig. 14. Part of the success of collapsing the data using $-P_G$ is the fact that the pressure distributions are relatively flat across the forward half of the collar surface, as shown in Fig. 6, where the bulk of the side force is distributed. The advantage of developing a design law based on $-P_G$ is that a priori knowledge of the collar pressure distribution is not required.

One of the inherent limitations of counterflow control is that the side forces necessary to vector thrust are generated by the distribution of vacuum pressures along the jet shear layer. Consequently, the design of any counterflow thrust vector system must assume that the maximum available differential pressure would occur when $-P_G$ is equal to atmospheric pressure P_∞ (i.e., absolute vacuum). Although establishing this condition is unlikely, it can be used to predict a lower bound on collar length necessary to vector thrust to a given δ_v. Using the expression given in Eq. (2), and rewriting ρU_1^2 as $\gamma P_\infty M^2$, valid for isentropic acceleration, the following relationship can be developed:

$$L_{\min}/H = \gamma M^2 \sin \delta_v \tag{3}$$

For the rectangular geometry examined in this study at a Mach number of 0.5, the minimum collar length would be approximately $L_{\min}/H = 0.12$, to achieve a thrust vector angle of 20 deg.

The ability to develop the required side forces to vector thrust will depend on a number of parameters that have not been examined parametrically in this study. In particular, the choice of a sectored-arc collar is not necessarily optimal, and was chosen here strictly for its geometric simplicity. One can anticipate that greater side forces may be created using elliptic or compound collar geometries. Furthermore, the development of the pressure distribution on the collar is a consequence of a pressure drop along the secondary flow path created between the collar surface and the primary jet shear layer. If this pressure drop was entirely because of the reversible flow acceleration along the collar, then the maximum possible differential pressure along the collar would be given by the isentropic choked flow conditions, setting a limit of $-P_G \approx 0.53P_\infty$. Since we can expect that there will be stagnation pressure loss along the secondary flow path, the maximum possible differential pressure across the collar will exceed $0.53P_\infty$. Hence, increasing the frictional effect experienced by the secondary counterflow will help to further increase the differential pressure and

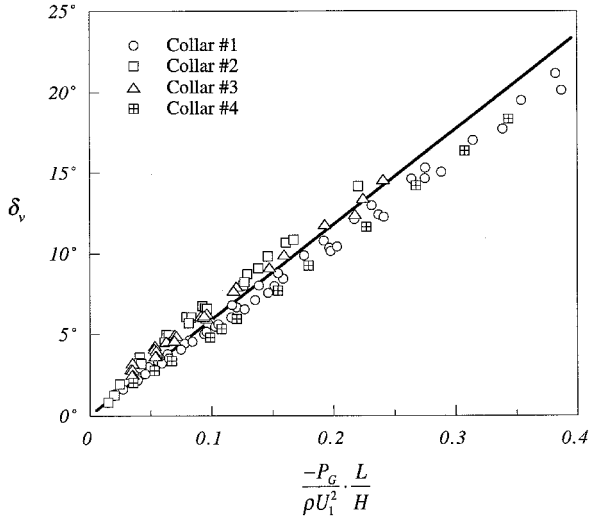

Fig. 14 Summary thrust vector response data for collars no. 1, 2, 3, and 4. Data obtained for gap heights between $0.2 \leq G/H \leq 1$ and Mach numbers between $0.32 \leq M_1 \leq 0.50$. Collar lengths also varied as indicated in Table 1.

the side force. Roughening the collar surface may serve this purpose nicely. Finally, the reader is reminded that performance of a fluidic-based control strategy must be examined for possible hysteretic effects. Demonstrating that the jet responds proportionally to collar pressure $-P_G$ is not proof that the flow is free of hysteresis effects, i.e., one must also identify $\delta_{v,\text{crit}}$ and operate at thrust vector angles below this value. Developing a model to predict jet attachment is necessary to apply the design curve over the intended operating domain. Future work must also assess the dynamic jet characteristics in the presence of counterflow.

Summary and Conclusions

The implementation of fluidic control to vector thrust of high-performance aircraft is attractive owing to the potential for fast time response and the reduced weight because of the elimination of actuation and control hardware currently used to vector thrust mechanically. Fluidic control, however, has not proven itself flight worthy, principally because of the inherent hysteretic nature of the control. In this study, fluidic control using counterflow was examined and found to perform free of bistable effects over portions of the operating domain. The most important parameter influencing jet attachment and the associated hysteresis was the length of the collar surface L. At a Mach number of 0.5, hysteresis-free performance could be achieved up to thrust vector angles of 20 deg for collar lengths of $L/H = 1$. If the collar length was increased to $L/H = 2$, then hysteresis effects were eliminated only up to thrust vector angles near 6 deg. When hysteresis could be avoided, the jet responded nearly linearly to the vacuum pressure developed in the counterflowing stream. Data taken during linear control, over a wide range of flow conditions and collar geometries, could be scaled using the momentum flux of the primary jet and the parameter L/H, where L is the streamwise extent of the collar surface and H is the short dimension of the rectangular jet.

Designing an efficient thrust vector system based on counterflow must consider a number of factors. The collar must be long enough to provide an extended surface over which the side forces can act to vector thrust, but not too long that the system will be plagued by hysteresis effects. Furthermore, the height of the secondary flow path must be kept as small as possible, because large gap heights G/H will result in increased secondary flow requirements as well as increased base drag associated with the downstream projected area of the collar operated at vacuum pressures. Finally, the counterflow system

will demand an on-board vacuum source, which may be accommodated using, for instance, an ejector nozzle, but considerations to overall system performance must be assessed before full integration can be completed.

Finally, some discussion is warranted concerning the extension of the present results to supersonic and high-temperature jet exhaust. As described earlier, continuous thrust vector control is possible because of the unique relationship between shear-layer velocity ratio and entrainment. Under realistic jet operating conditions, one must also consider the independent effects of density ratio and compressibility on the shear-layer dynamics. Papamoschou and Roshko[23] demonstrated, for instance, that shear-layer growth rates will decrease with increasing convective Mach number (increasing levels of compressibility) and increase as the jet density is reduced (jet temperature is increased) relative to the surrounding fluid. At all convective Mach numbers and density ratios, however, the shear-layer entrainment rate will increase monotonically with velocity ratio. Evidence of this relationship was recently demonstrated at compressible flow conditions in a Mach 2 jet over a range of density ratios.[20] Hence, there appears to be no limitation to thrust vector control using counterflow based on changes in compressibility and density ratio across the shear layer. This expectation is borne out, at least over a limited range of supersonic flow conditions, in a recent study by Strykowski et al.,[24] where pitch vector control using counterflow was investigated at freestream Mach numbers up to 2 in both hot and cold jet exhausts. These authors demonstrated that thrust vector angles up to approximately 20 deg could be achieved in supersonic jets with secondary mass flow requirements less than 2% of the primary jet mass flow.

Acknowledgments

The authors would like to express their thanks to the National Science Foundation, Contract CTS-9116532, and the Air Force Office of Scientific Research, Contract F49620-94-1-0046, for financial support of this research. We also benefited considerably from discussions with G. Schmid of the University of Minnesota, and F. Alvi and A. Krothapalli of Florida State University.

References

[1]Mishler, R., and Wilkinson, T., "Emerging Airframe/Propulsion Integration Technologies at General Electric," AIAA Paper 92-3335, July 1992.

[2]Capone, F., Smereczniak, P., Spetnagel, D., and Thayer, E., "Comparative Investigation of Multiplane Thrust Vectoring Nozzles," AIAA Paper 92-3264, July 1992.

[3]Henderson, W. P., "Propulsion Systems Integration in High Performance Aircraft," *Aerospace Engineering*, Vol. 10, No. 2, 1990, pp. 21–25.

[4]Doonan, J. G., and Kuchar, A. P., "Scale Model Test Results of a Multi-Slotted 2-D/C-D Ejector Nozzle," AIAA Paper 92-3264, July 1992.

[5]Snow, B. H., "Thrust Vectoring Control Concepts and Issues," Society of Automotive Engineers Technical Paper Series, 901848, Oct. 1990.

[6]Bursey, R. N., Berger, C. W., and DeFreese, C. G., "Pratt & Whitney Vectoring Team Turns Imagineering into Reality," Pratt & Whitney Government Engines and Space Propulsion Paper, West Palm Beach, FL, Nov. 1993.

[7]Olsen, R. E., "Reattachment of a Two-Dimensional Compressible Jet to an Adjacent Plate," American Society of Mechanical Engineers Symposium on Fluid Jet Control Devices, Nov. 1962.

[8]Comparin, R. A., Mitchell, A. E., Mueller, H. R., and Glaettli, H. M., "On the Limitations and Special Effects in Fluid Jet Amplifiers," American Society of Mechanical Engineers Symposium on Fluid Jet Control Devices, Nov. 1962.

[9]Warren, R. W., "Some Parameters Affecting the Design of Bistable Fluid Amplifiers," American Society of Mechanical Engineers Symposium on Fluid Jet Control Devices, Nov. 1962.

[10]Gilbert, B., "Directional Control of Large Mass Flows by Fluidics," FLUCOME '91, American Society of Mechanical Engineers 3rd Triennial International Symposium of Fluid Control, Measurement, and Visualization, Aug. 1991.

[11]Fitzgerald, R. E., and Kampe, R. F., "Boundary Layer TVC for Missile Applications," AIAA Paper 83-1153, June 1983.

[12]Carrol, G. R., and Cox, H., "A Missile Flight Control System Using Boundary Layer Thrust Vector Control," AIAA Paper 83-1149, June 1983.

[13]Porzio, A. J., and Franke, M. E., "Experimental Study of a Confined Jet Thrust Vector Control Nozzle," *Journal of Propulsion and Power*, Vol. 5, No. 5, 1989, pp. 596–601.

[14]Squire, H. B., "Jet Flow and Its Effect on Aircraft," *Aircraft Engineering*, Vol. 22, March 1950, pp. 62–67.

[15]Wilson, D. J., "An Experimental Investigation of the Mean Velocity, Temperature and Turbulence Fields in Plane and Curved Two-Dimensional Wall Jets: Coanda Effect," Ph.D. Dissertation, Univ. of Minnesota, Minneapolis, MN, Dec. 1970.

[16]Young, T., "Outlines of Experiments and Inquiries Respecting Sound and Light," Lecture to the Royal Society, Jan. 1800; also *Journal of the Royal Aeronautical Society*, Vol. 61, 1957, p. 157.

[17]McGlaughlin, D. W., and Greber, I., "Experiments on the Separation of a Fluid from a Curved Surface," *Advances in Fluidics*, American Society of Mechanical Engineers, New York, 1967, pp. 142–161.

[18]Van der Veer, M. R., "Counterflow Thrust Vectoring of a Subsonic Rectangular Jet," M.S. Thesis, Univ. of Minnesota, Minneapolis, MN, 1995.

[19]Brown, G. L., and Roshko, A., "On Density Effects and Large Scale Structure in Turbulent Mixing Layers," *Journal of Fluid Mechanics*, Vol. 64, Pt. 4, 1974, pp. 775–816.

[20]Strykowski, P. J., Krothapalli, A., and Jendoubi, S., "The Effect of Counterflow on the Development of Compressible Shear Layers," *Journal of Fluid Mechanics*, Vol. 308, Feb. 1996, pp. 63–96.

[21]Strykowski, P. J., and Wilcoxon, R. K., "Mixing Enhancement Due to Global Oscillations in Jets with Annular Counterflow," *AIAA Journal*, Vol. 31, No. 3, 1993, pp. 564–570.

[22]Drazin, P. G., and Reid, W. H., *Hydrodynamic Stability*, Cambridge Univ. Press, Cambridge, England, UK, 1981.

[23]Papamoschou, D., and Roshko, A., "The Compressible Turbulent Mixing Layer: An Experimental Study," *Journal of Fluid Mechanics*, Vol. 197, Dec. 1988, pp. 453–477.

[24]Strykowski, P. J., Krothapalli, A., and Forliti, D. J., "Counterflow Thrust Vectoring of Supersonic Jets," *AIAA Journal*, Vol. 34, No. 11, 1996, pp. 2306–2314.